ACS APPLIED MATERIALS & INTERFACES

Research Article

www.acsami.org

Photochromic Organic Nanoparticles as Innovative Platforms for Plasmonic Nanoassemblies

Kristen E. Snell,[†,§] Jean-Yves Mevellec,[‡] Bernard Humbert,[‡] François Lagugné-Labarthet,[§] and Eléna Ishow*,[†]

[†]CEISAM−UMR CNRS 6230, Université de Nantes, 2 rue de la Houssinière, 44322 Nantes, France

[‡]IMN−UMR CNRS 6502, Université de Nantes, 44322 Nantes, France

[§]Department of Chemistry, University of Western Ontario, 1151 Richmond Street, London, Ontario N6A5B7, Canada

Supporting Information

ABSTRACT: The fabrication of hybrid core−shell nanoassemblies involving a nondoped azo photochromic core coated with a dense shell of gold nanoparticles is reported to investigate the influence of localized plasmons onto the azo core photoisomerization. Photochromic organic nanoparticles, regarded as a novel class of high-density photoswitchable nanomaterials, are first elaborated upon precipitation in water of push−pull azo molecules, containing sulfur-terminated units to chelate gold nanoparticles. Photoisomerization studies of the azo nanoparticles reveal significantly higher $E \rightarrow Z$ photoconversion yields and $Z \rightarrow E$ thermal back relaxation rate constants compared to those of dyes processed as thin films and in solution, respectively. These unexpected results are ascribed to the large surface-to-volume ratio and cooperative effects encountered in nanoparticles that deform without disassembling under polarized illumination as a result of the weak change in the azo dipole moment. UV−vis spectroscopy and Raman microscopy of the hybrid nanoassemblies show strong optical coupling between both photoactive constituents, confirming that gold nanoparticles are tightly positioned on the azo core surface. Such coupling causes partial quenching of the azo photoisomerization but does not impact the thermal back relaxation. Longer sulfur-terminated chains provide reduced quenching of the photoreaction by the localized plasmons, thereby opening perspectives toward plasmon-mediated deformation of nano-objects for light-controlled nanomechanics.

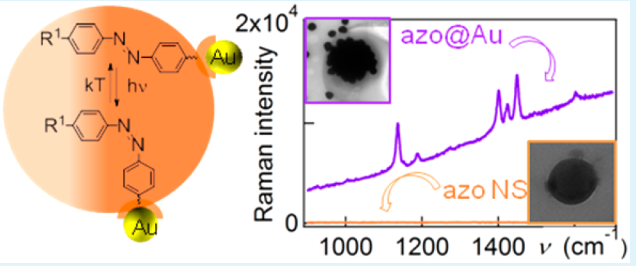

KEYWORDS: *azo materials, hybrid nanoparticles, photochromism, photodeformation, Raman spectroscopy, plasmonics*

INTRODUCTION

Hybrid nanomaterials combining organic photoactive units and plasmonic nanoparticles have gained considerable interest in the fields of data storage, photovoltaics, biosensing, chemical reactivity and drug release, to cite only a few.[1−4] Particular attention has very recently been devoted to the combination of inorganic nanoparticles (silver or gold) and photochromes,[5,6] amenable to undergo reversible changes in the absorption spectra and geometries upon light absorption. In this way, the mutual interplay between organics and metal properties can be used to finely tune the photochrome reactivity as well as the energy of the localized surface plasmon resonance (LSPR) of the metallic nanoparticles.[7,8] As photochromic molecules react in the picosecond range,[9−13] strong optical coupling between their excited states and the LSPR collective electron oscillation must operate. This requires a subtle balance in terms of distance,[14−16] size[17] or shape[18] of the plasmonic nanoparticles with respect to the photochromes to match their electronic transitions. Most of the studies reported so far deal with grafted diarylethene[15,19−21] and spiropyrane[22,23] derivatives, characterized by an initial colorless state and a colored photoreacted state that causes an energy shift of the LSPR band in a privileged manner. By contrast, only a few examples have reported the combination of azo photochromes with plasmonic nanoparticles. Azo derivatives, undergoing reversible *E-Z* photoisomerization, are known for their large light-triggered changes in geometry and polarity.[24] These photoinduced changes have been advantageously exploited to move external macroscopic objects[25−27] but appeared to be very troublesome for azo-functionalized metallic nanoparticles.[28] The latter nano-objects indeed tend to collapse after illumination into supraparticles that could smartly modulate the LSPR upon nanoparticle aggregation.[29,30] Even though these phenomena due to unstable solvation interactions with the surrounding organic phase are reversible, an inevitable association occurs under light activation, which impairs comprehensive analyses of the influence of surface plasmons onto the azo photoisomerization.[31] Azo-functionalized polymers deposited on plasmonic structures have also been used to indirectly map the optical near-field confined around individual or pairs of

Received: November 5, 2014
Accepted: January 5, 2015
Published: January 5, 2015

DOI: 10.1021/am5076953
ACS Appl. Mater. Interfaces 2015, 7, 1932−1942

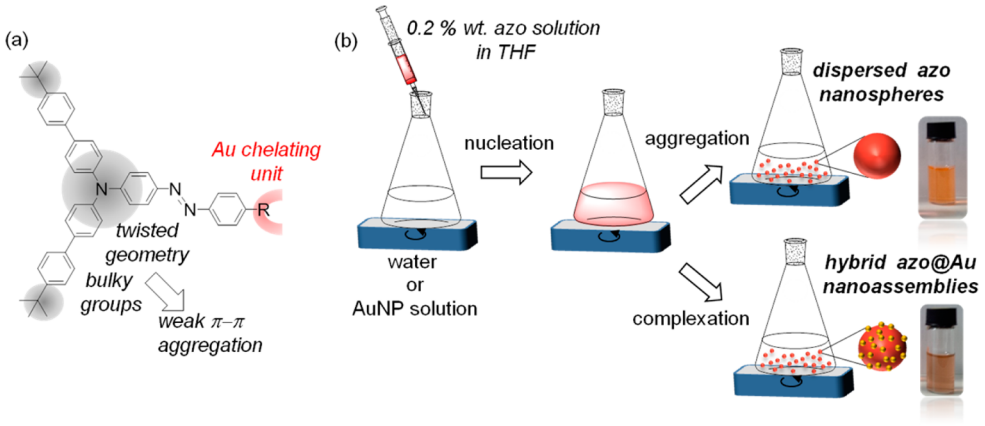

Figure 1. (a) Generic backbone of the molecular azo precursors forming the azo nanoparticles and hybrid azo@Au nanoassemblies. (b) Schematic description of the fabrication of azo nanospheres and azo@Au nanoassemblies upon reprecipitation and self-assembling of azo derivatives in water or in gold colloidal suspensions after quick addition of an azo solution in tetrahydrofuran (THF) solution (0.2 wt %).

metallic nanoparticles.[17,32−34] However, the search for hybrid azo nanostructures that are stable in solution after illumination still represents a current challenge. Moreover, photophysical characterizations in nanoassemblies that respect the individual molecular architecture in diluted solutions require a high payload of photoreactive units per nanoassembly to obtain detectable spectral modifications. A novel class of high-density organic nanomaterials has thus emerged, made exclusively of self-assembled small functional molecules.[35] Compared to the traditional approach consisting of latex and inorganic matrices functionalized with molecular photochromes,[36] photochromic organic nanoparticles are characterized by a higher payload of photoswitchable molecules that can give rise to cooperativity effects upon photoreaction due to strong conformational confinement.[37] They are advantageously obtained following a simple reprecipitation process from concentrated dye solutions (bottom-up)[38] or a more sophisticated laser ablation method using partly soluble materials at the initial stage and stabilizing surfactants (top-down).[12,39] On the other hand, the design of photochromic units has to meet stringent photophysical and geometrical criteria, such as enough free volume, absence of $\pi-\pi$ stacking that impedes efficient photoreaction of the closely lying photoactive units, and optical matching of the LSPR resonance with the irradiation wavelength responsible for the photoisomerization reaction. It is thus no coincidence that most of the regarded photochromic nanoparticles involved diarylethene derivatives, known to undergo restricted backbone reorganization after photoreaction. Those involving azo compounds face dissociation into their molecular units upon *E*-*Z* isomerization[40,41] because the latter process requires significant space and destabilizes the whole structure. To respond to the lack of stable azo nanoparticles upon illumination, we herein report on the synthesis of a series of amorphous push−pull molecular azo materials containing bulky substituents to permit photoreaction in the solid state and forming stable colloidal photoswitchable nanoparticles. The introduction of sulfur-terminated chains linked to the azo backbone allows us to generate unexplored core−shell plasmonic hybrid nanoarchitectures azo@Au upon simple ligand exchange at the interface between the azo organic nanoparticles and gold nanoparticles. Functional nanostructures comprising a shell of plasmonic or magnetic nanoparticles have recently emerged as promising materials in theranostics as high density active materials allow efficient hyperthermia effects and imaging contrast to be achieved at much lower injected doses compared to a dispersion of individual nanoparticles.[2,42,43] Photochromic nanoplatforms, carrying a shell of gold nanoparticles, could represent attractive architectures to trigger the optical response of the shell using light only. The absence of surfactant during the fabrication process provides for the first time clear-cut evidence on the remarkable properties of photochromic nanoparticles, found to be intermediate between those of azo solutions and nondoped nanometric films. Strong optical coupling between the azo derivatives of the core and the shell of gold nanoparticles is unambiguously demonstrated by Raman microscopy and photochromic measurements that show unexpected dependence of the length of the sulfur chelating chain.

RESULTS AND DISCUSSION

Elaboration of Photochromic Nanoparticles. The targeted azo derivatives, noted azoS$_2$, azo6-SAc and azo11-SAc, contained a twisted triphenylamino center as well as bulky peripheral *tert*-butylphenyl substituents to bring enough free volume when self-assembled as nanoparticles or processed as thin films. In this way, undesirable $\pi-\pi$ stacking blocking the photoisomerization process is avoided (Figure 1).

They additionally displayed a push−pull backbone involving an electron-donating triphenylamino unit and an electron-accepting ester moiety. As exposed below, the resulting charge transfer appears to be essential to stabilize the corresponding nanoparticles containing both *E* and *Z* azo isomers states through strong dipole−dipole interactions with the surroundings. Finally, the fabrication of innovative plasmonic assemblies consisting of a photochromic core coated with gold nanoparticles led us to integrate sulfur-based coordinating units like disulfide and thioacetate, showing strong affinity toward gold surface and avoiding a mixture of oxidized and reduced forms when using alkanethiols. The length of the alkyl chain separating the sulfur unit from the azo moiety was varied from six to eleven carbon atoms to investigate the hydrophobic/hydrophilic balance onto the azo nanoparticle formation and the evolution of the photochromic properties. To this aim, the same azo carboxylic intermediate was employed and transformed either into a more reactive acyl chloride or activated using a carbodiimide agent to yield the corresponding azo esters azoS$_2$, azo6-SAc and azo11-SAc (Figure 2). It is

DOI: 10.1021/am5076953
ACS Appl. Mater. Interfaces 2015, 7, 1932−1942

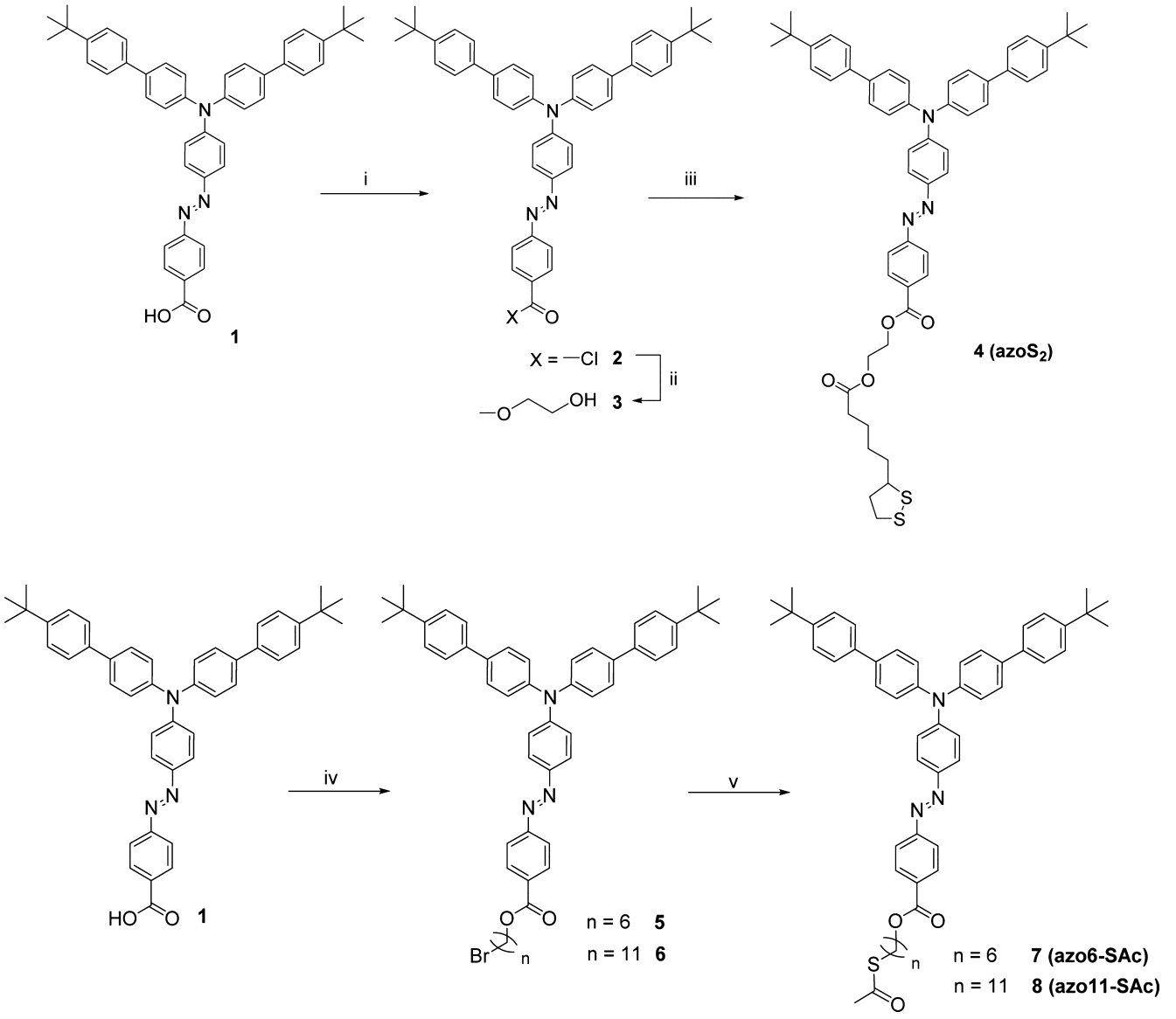

Figure 2. Synthetic pathway toward the gold nanoparticle chelating azo derivatives $azoS_2$ (**4**), azo6-SAc (**7**) and azo11-SAc (**8**). (i) Thionyl chloride; CH_2Cl_2 reflux, 4 h; (ii) ethylene glycol, CH_2Cl_2 reflux, 18 h, 56%; (iii) lipoic acid, diisopropylcarbodiimide (DIPC), 4-dimethylaminopyridinium *p*-toluenesulfonate (DPTS), CH_2Cl_2, 0−25 °C, 2 days, 90%; (iv) 6-bromohexan-1-ol or 11-bromoundecan-1-ol, DIPC, DPTS, CH_2Cl_2, 0−25 °C, 2 days, 82−85%; (v) potassium thioacetate, acetone, RT, 18 h, 90−95%.

worth mentioning that the mild Steglich esterification failed in the case of $azoS_2$, yielding intractable byproducts.

Azo nanoparticles were obtained for all compounds by quickly adding into an excess of Millipore water (2.5 mL) a 0.2 wt % azo solution in THF (50 μL). These conditions revealed to be the best ones in terms of compound solubility and nanoparticle formation that obeys a recently demonstrated regime of nucleation-aggregation, valid for metallic[44] and organic nanoparticles.[45] Their size distribution was characterized by dynamic light scattering (DLS) and transmission electron microscopy (TEM) using no specific staining (Figure 3).

Both techniques showed a larger mean diameter for azo11-SAc at 139 ± 20 nm, despite a slightly lower concentration, compared to those for azo6-SAc (125 ± 48 nm) and $azoS_2$ (90 ± 31 nm). This evolution is coherent with the higher hydrophobic character brought by the alkane chain for azo11-SAc and azo6-SAc compared to $azoS_2$, which contains a hydrophilic ethylenoxy fragment. Indeed, the injection into water of solutions of hydrophobic molecules leads to a high amount of nuclei that merge into larger nanoparticles upon aggregation.[46] Interestingly, the surface potentials ζ were found highly negative for all compounds at the same value of −40 mV, and were attributed to strong dipole−dipole interactions between the polar water molecules and azo dyes at the nanoparticle surface and the adsorption of trace carboxylic acids as contaminants.[47] Such high values spare us from using stabilizing surfactants that can significantly impair the photoisomerization process of azo nanomaterials.

Photoisomerization of Photochromic Azo Nanoparticles. As the samples revealed to be very sensitive to ambient light, the corresponding solutions were carefully prepared in the dark while all thin films (prepared by spin-coating a 2 wt % azo solution in chloroform onto precleaned glass substrates) were stored in the dark for several days before studying. Irradiation at 488 nm (8 mW·cm^{-2} provided by a white light source equipped

DOI: 10.1021/am5076953
ACS Appl. Mater. Interfaces 2015, 7, 1932−1942

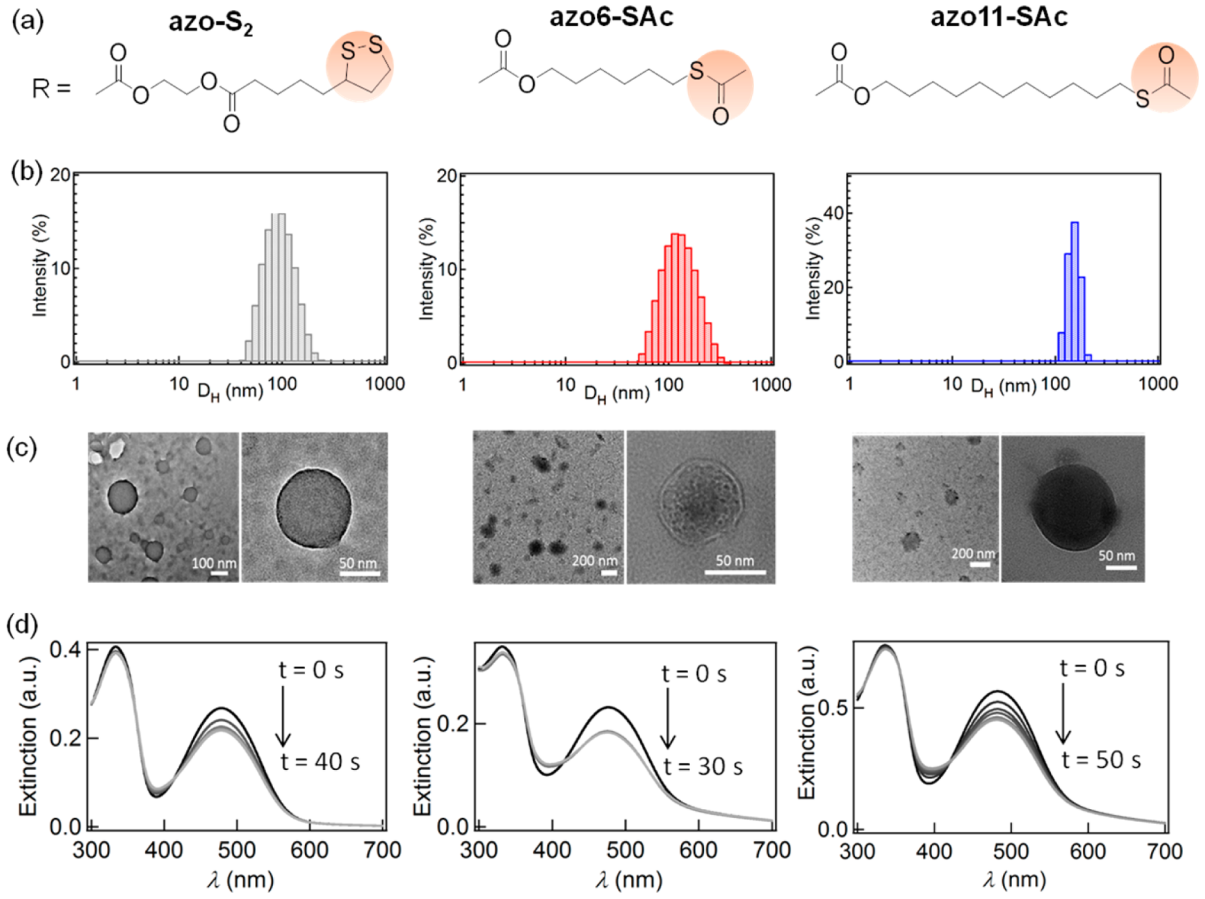

Figure 3. (a) Structure of the gold-chelating units R for azo-S_2, azo6-SAc and azo11-SAc whose main backbone is defined in Figure 1. (b) DLS measurements of the mean hydrodynamic diameter D_H of azo nanospheres after adding a 0.2 wt % azo solution in THF (50 μL) into water (2.5 mL) (azo-S_2, D_H = 90 ± 31 nm; azo6-SAc, D_H = 125 ± 48 nm; azo11-SAc, D_H = 139 ± 20 nm). (c) TEM imaging. (d) Evolution of the absorption spectra of azo nanosphere solutions upon irradiation at 488 nm (8 mW·cm^{-2}); each spectrum was obtained every 10 s of irradiation until the photostationary state was reached.

Table 1. UV-vis Absorption and Photochromic Properties of azo-S_2, azo6-SAc and azo11-SAc in Toluene Solution (TOL), Self-Assembled as Nanoparticles (NP) and Processed as Thin Films, and Solutions of azo@Au Nanoassemblies in Water

	λ_{max}(abs) (nm)			ρ (%)[d]			k_i (f_i) (10^{-5} s^{-1})[e]		
compounds	TOL[a]	NP[b]	films[c]	TOL	NP	films	TOL	NP	films
azo-S_2	471	480	479	50	21	13	6.7	13	5.8 (92.5)
	331	333	328						30.1 (7.5)
azo6-SAc	467	477	473	46	22	14	7.4	10.5	3.5 (97.5)
	330	331	329						31.8 (2.5)
azo11-SAc	467	483	478	49	21	15	7.6	11.3	8.7 (86.5)
	330	337	335						25.6 (13.5)
azoS_2@Au		510			9.2			12.3	
		331							
azo6@Au		514			8.3			10.3	
		324							
azo11@Au		506			13			9.5	
		333							

[a]Solution in toluene (3×10^{-5} mol·L^{-1}). [b]Obtained after addition into Millipore water (2.5 mL) of a 0.2 wt % azo solution in THF (50 μL). [c]From spin-coating a 2 wt % azo solution in chloroform. The thickness d was measured to be around 250 nm except for azo11-SAc where d = 700 nm. [d]Minimal conversion yield $\rho = (A_0 - A_{PSS})/A_0$, where A_{PSS} and A_0 designate the absorbances at the photostationary state and before irradiation, respectively, and considering that the Z isomers do not absorb. [e]Experimental fit of the recovered absorbance of the E species upon back thermal relaxation in the dark. Monoexponential law for solutions and nanosphere suspensions, and biexponenial law for thin films. For these latter, the fraction f_i associated with the rate constant k_i is defined as $f_i = k_i/\sum_j k_j$.

with a bandpass filter) in the visible absorption band related to an azo-spread $\pi\pi^*$ transition caused strong decrease of the charge transfer band due to $E \rightarrow Z$ photoisomerization (Figure 3d). No nanoparticle aggregation was observed as noticed from

DOI: 10.1021/am5076953
ACS Appl. Mater. Interfaces 2015, 7, 1932−1942

the almost unchanged absorbance baseline at longer wavelengths. Compared to dyes dissolved in toluene or processed as thin films, the azo nanoparticles exhibited intermediate minimum $E \rightarrow Z$ photoconversion yields ρ valued at 21−22% (Table 1).

Indeed, the ρ values dropped dramatically from 46 to 50% in constraint-free solutions to only 13−15% for 200 nm-thick films. As all systems exhibit isotropic distribution of the dyes, specific molecular arrangements can be discarded to explain the superior photoconversion yields of azo nanoparticles compared to those of azo thin films. TEM analyses actually revealed no diffraction patterns while all thin films displayed a glassy aspect with no microcrystalline traces at room temperature. Moreover, thermal measurements of the powder, using differential scanning calorimetry, showed no melting point while glass transition temperatures T_g could be measured after a first heating−cooling cycle. The notable decrease in the glass transition temperature for azo11-SAc (T_g = 40 °C) compared to those for azo6-SAc (T_g = 59 °C) and azoS_2 (T_g = 63 °C) features lesser dipolar interchain interactions, which confirms the higher degree of hydrophobicity of the C11 alkyl chains as the main parameter responsible for the larger size of azo11-SAc nanoparticles.

The photochromism studies of the back thermal reaction $Z \rightarrow E$ for the nanoparticles also revealed to be very counterintuitive in terms of kinetic models and rate constant values. Two cycles of photoirradiation-relaxation showed a fully reversible mechanism (see the Supporting Information, Figure S1). Azo compounds are indeed known as T-photochromes and revert back to their initial state in the dark under thermal activation over a time range of a few seconds to a few days depending on their structure. The thermal relaxation could be fitted with a monoexponential mathematical law not only for azo solutions but also for nanoparticles. The behavior of nanoparticles thus contrasts with that of thin films whose relaxation modeling requires a biexponential law, as commonly evoked to explain distinct trapped geometries in the ground state[48,49] as well as in the excited state.[50] Moreover, the rate constants k were found higher for nanoparticles at around 11−13 × 10^{-5} s^{-1} against 6.7−7.6 × 10^{-5} s^{-1} for toluene solution whereas the overall relaxation in thin films was globally slower, except for azo11-SAc due to a higher thickness, making the comparison more delicate. A first explanation could be related to the high density of photochromes in the nanospheres, so that the spontaneous relaxation of one molecule cooperatively accelerates the relaxation of the surrounding molecules. A second interpretation is likely to be found in the much higher surface-to-volume ratio exhibited by the photochromic nanoparticles with regard to those of 2D nanometric surfaces. Polarity effects due to the water molecules (ε_r = 78.5 D) at the nanosphere surface could also play an additional role as polar solvents are known to accelerate the $Z \rightarrow E$ back thermal relaxation kinetics of push−pull azo compounds.[11,51] The absorption maxima were indeed found at higher wavelengths for azo nanospheres (477−483 nm) compared to azo solutions in toluene (467−471 nm). Both assumptions tend to suggest that the photoisomerization reaction proceeds from the surface and propagates to the core as the molecules at the interface exhibit weaker constraints than those in the core. Such observation is to be related to aqueous suspensions of fluorescent organic nanoparticles (FON) whose emission signal is often dramatically quenched by vibrational coupling with the water molecules located at the interface that contributes the most to the global emission intensity.[52−54] The effect of interfacial interactions is actually of utmost importance. It is, however, noteworthy that the monoexponential relaxation kinetics found for the photochromic nanoparticles strongly differ from the multiexponential fluorescence decays evidenced for fluorescent nanoparticles, which was ascribed to a structural heterogeneity arising from the nucleus aggregative mechanism ruling the nanoparticle growth.[45] As the spectroscopic studies of photoactive organic nanoparticles have been overlooked so far, such important observations request further thorough time-resolved photophysical studies at the nanoscale, that are beyond the scope of the current studies.

Remarkably, no dissociation of the irradiated azo nanoparticles occurred, as proved by the complete recovery of the initial absorbance and the absence of hypsochromic shift of the absorption maximum after back thermal relaxation. Free dyes in solution actually absorb at around 467−471 nm against 477−483 nm for nanoparticle suspensions. Such remarkable stability must originate from the low change in dipole moment between the E (4.91 D) and Z (4.78 D) forms as computed using time-dependent functional theory (BY3LP functional and 6-31G(d) basis set), hence the nanoparticle surface undergoes stabilizing dipole−dipole interactions with the surrounding water molecules. By contrast, most of the azo derivatives investigated in the literature, forming molecular nanoparticles or self-assembled vesicles, were made of mono- or dialkoxy substituted azobenzenes, regarded as weakly polar structures.[40,55,56] They were reported to markedly collapse in organic solvents or disassembled in aqueous solutions organic as a result of the large increase in their dipole moment upon photoisomerization (from 0 to 1.2 D for the E isomer to 3.2−4.9 D for the Z isomer).[57,58] This polarity change would indeed correspond to the replacement of carbon tetrachloride with acetone. In our case, DLS measurements right after photoirradiation showed slight size shrinkage for azoS_2 and azo6-SAc nanoparticles that could be attributed to the azo backbone contraction upon E to Z transformation. The opposite trend was found for azo11-SAc along with an increase in the size distribution, likely due to the larger size of the alkyl chain, giving rise to a more disorganized structure after illumination (as already showed by a lower T_g in the E configuration compared to those of azo6-SAc and azoS_2). Nevertheless, TEM measurements could not evidence significant size changes of nanoparticles before and after isomerization given the relatively broad size distribution. We thus used the linearly polarized beam of an argon ion laser working at 488 nm (470 mW·cm^{-2}) and irradiated the entire area of a TEM grid (Ø = 3 mm), placed vertically and covered with a droplet of an aqueous suspension of azo11-SAc nanoparticles. Once the droplet has dried (after ∼30 min of irradiation), TEM imaging was immediately performed (Figure 4).

Most of the initially spherical nanoparticles adopted a croissant-like geometry, recalling the uniaxial deformation reported for azo polymer nanoparticles subjected to polarized illumination.[59] The random orientation of the "croissants" instead of being unidirectional is to be attributed to the Browian motion of the nanoparticles, freely rotating in the water droplet at room temperature. Interestingly, no deformation could be observed for dried samples here, contrarily to azo polymer nanoparticles where the azo moieties were grafted as side chains of a polyether backbone.[60] This observation confirms the prevailing role of the nanoparticle

DOI: 10.1021/am5076953
ACS Appl. Mater. Interfaces 2015, 7, 1932−1942

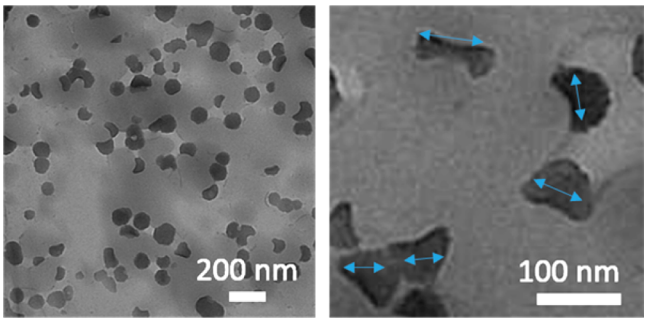

Figure 4. TEM imaging of azo11-SAc nanoparticles deposited on a TEM copper grid after irradiation at 488 nm using a linearly polarized light (470 mW·cm^{-2}, 30 min, Ar^+ laser) until the colloidal suspension dried.

interface and interactions with the dynamic shell of solvation in the photoisomerization process.

Hybrid Core−Shell azo@Au Nanoassemblies. The stiff cohesion of the investigated azo nanospheres and their ability to photoisomerize prompted us to explore original core−shell architectures, comprising an azo nanocore coated with gold nanoparticles (AuNP) in order to tune the photoinduced nanosphere deformation by gold nanoparticles located at their surface. We first synthesized hydrophilic AuNP (Ø = 15 ± 3 nm) using Turkevich's method, based on the reduction of the tetrachloroaurate $HAuCl_4$ salt by citrate ions that also act as stabilizing and easily exchangeable capping ligands. The hybrid nanoassemblies were simply obtained by injecting organic azo solutions in THF into a freshly prepared suspension of gold nanoparticles following the same protocol as that earlier described for neat organic photochromic nanoparticles. After several hours or days under stirring to let the ligand exchange process occur, stable azo@Au nanoassemblies were formed with no decantation over time. They displayed a dense shell of highly contrasted gold nanoparticles organized around the organic nanosphere, as evidenced by 2D-TEM imaging. The strong affinity of the disulfide and thioacetate groups toward gold favorably displaces the capping citrate ligands that continue to stabilize the gold nanoparticle outer part, nonchelated by the central azo nanoplatform. DLS measurements evidenced a slight increase in the mean hydrodynamic diameter and the size dispersion as expected from the grafting of gold nanoparticles. Remarkably, very few uncomplexed gold nanoparticles were left as proved by the small amplitude of the corresponding peak (10−20 nm) on the DLS intensity histogram and the low amount of isolated gold nanoparticles on TEM images (Figure 5).

Optical Coupling Characterization Using Raman Microscopy. By assuming a tight monolayer coverage of gold nanoparticles, one could estimate that a 120 nm large azo nanosphere would be coated with about 250 gold nanoparticles. The absorption spectra of the azo@Au nanoassemblies exhibited the typical azo charge transfer band whose maximum was yet artificially displaced at 506−510 nm due to the local surface plasmon resonance (LSPR) contribution of AuNP peaking at 528 nm. It is worth noting that the absorption spectrum of the nanoassemblies slightly differs from the sum of the absorption spectra characteristic of each constitutive unit, taken independently (Figure 6a). The major discrepancy operates at the azo absorption band, featuring a possible optical coupling with the LSPR band as both occur at similar energies. Upon photoirradiation of the nanoassemblies at 488 nm in the same conditions as before, the band characteristic of the azo charge transfer decreased in intensity, albeit to a lesser extent than for neat organic nanospheres (Figure 6b).

The minimum photoconversion yields ρ reached only 8−13% against 21% for the organic nanospheres. Changing the excitation wavelength closer to the LSPR maximum at 547 or at 365 nm corresponding to the azo singlet excited state S_2 located at the biphenyl moieties did not improve ρ, and instead led to even more reduced values due to less population of the azo $\pi\pi^*$ reactive state. Conversely, almost no change in the rate constants k of the back thermal relaxation, calculated at 9.5−12 × 10^{-5} s^{-1}, could be observed between the free and gold-coated azo nanospheres that also showed full stability after irradiation. These observations demonstrate again the presence of a strong optical coupling between the azo excited state and the AuNP plasmon during the $E \rightarrow Z$ photoreaction despite the subpicosecond regime/dynamics of the azo photoisomerization process. The significantly higher ρ value for azo11-SAc@Au nanoassemblies may stem from the longer alkyl C11 chain insulating the azo core from the AuNP, and thus diminishing the plasmonic coupling that exponentially decreases according to the distance.[4] By contrast, the back thermal relaxation, taking

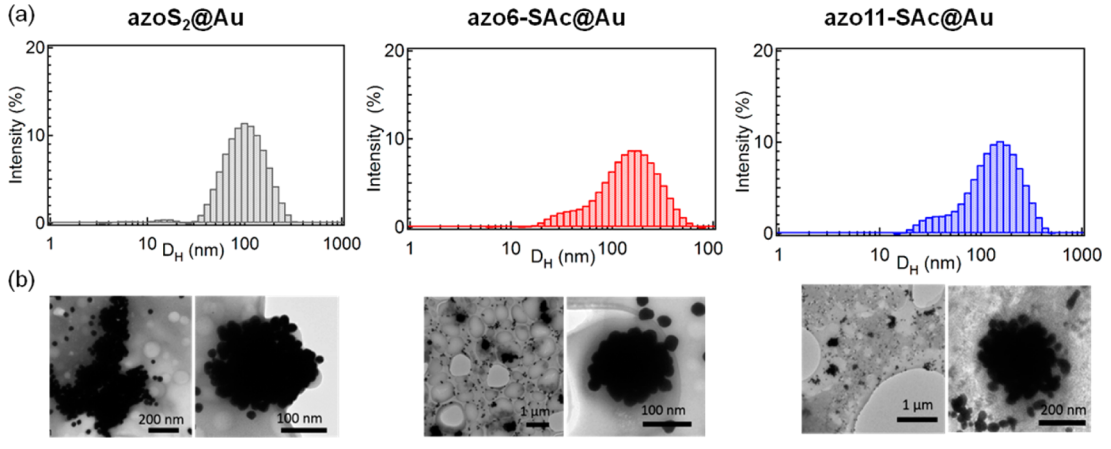

Figure 5. (a) DLS measurements of the mean hydrodynamic diameter D_H of azo@Au nanoassemblies comprising an azo core (azo-S_2, azo6-SAc or azo11-SAc) and a shell of gold nanoparticles capped with citrate anions (azo-S_2@Au, $D_{H=}$ 102 ± 47 nm; azo6-SAc@Au, $D_{H=}$ 156 ± 99 nm; azo11-SAc@Au, $D_{H=}$ 137 ± 77 nm). (b) TEM imaging.

DOI: 10.1021/am5076953
ACS Appl. Mater. Interfaces 2015, 7, 1932−1942

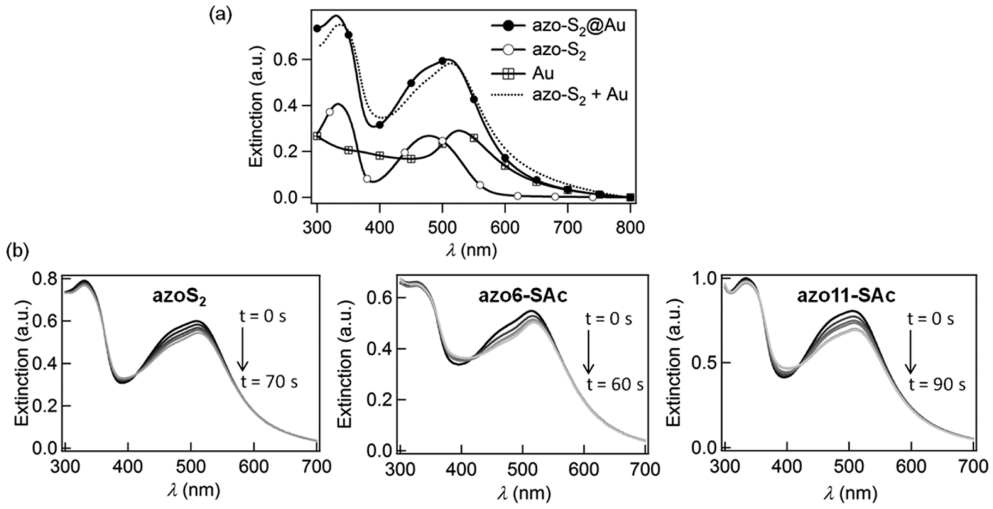

Figure 6. Photophysical characterizations of azo@Au nanoassemblies in Millipore water. (a) Comparative UV−vis absorption spectra of $azoS_2$@Au nanoassemblies, $azoS_2$ nanospheres, AuNPs and the artificial sum of independent $azoS_2$ nanospheres and AuNPs. (b) Evolution of the absorption spectrum upon irradiation at 488 nm (8 mW·cm^{-2}); each spectrum was obtained every 10 s of irradiation until the photostationary state was reached.

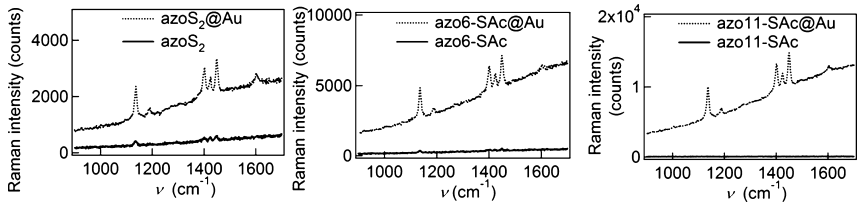

Figure 7. Raman spectra of $azoS_2$, azo6-SAc and azo11-SAc nanoparticles and the corresponding azo@Au nanoassemblies using a 514 nm laser excitation (15 W·cm^{-2} power, 1 s exposure time and 10 accumulations).

place in the dark, is only influenced by local polarity effects exerted by the surrounding molecules, which do not significantly vary between azo nanospheres and azo@Au nanoassemblies as the zeta potential was measured at −40 mV for both kinds of nano-object.

To assert further the gold NP anchoring onto the organic nanospheres and infer mutual optical interactions, Raman microscopy was used since it offers a high spatial resolution (i.e., ∼1 μm) together with a unique sensitivity to the vibrational fingerprints of the molecules of interest. Both azo@Au nanoassemblies and azo nanospheres, serving as models, were investigated. The use of gold nanoparticle in Raman spectroscopy is of great interest because both excitation and scattered electric fields are enhanced when the excitation and LSPR of the metallic particle energetically match, resulting in a very confined optical near-field.[61] Through such plasmon-mediated surface enhancement, the scattered Raman signal of closely lying organic materials has been reported to be amplified by 5 orders of magnitude.[62] In this work, four excitation wavelengths from the near-infrared to the visible range were employed: 785 or 633 nm (far from the AuNP LSPR absorption band), 514 nm (matching the absorption maximum wavelength of the AuNP LSPR band) and 488 nm close to the azo absorption band. At 785 and 633 nm, the vibrational stretching modes of the azo material composing the core of the hybrid nanospheres were hardly observed. Excitation at 488 nm induced a photoreaction, causing irreversible damages of the nano-object that was burned by the laser. We thus privileged the use of a laser excitation at 514 nm, operating at the power of 15 W·cm^{-2}, with an exposure time of 1 s and 10 accumulations. Contrary to previous studies reporting the impossibility to characterize classical arrangements where azo ligands were grafted on the surface of gold nanoparticles,[56] the azo@Au nanoassemblies clearly responded with an intense Raman signal in the 1400−1500 cm^{-1} range that was ascribed to the normal modes of elongation ν(N═N) and deformation δ(C═C) of the azo unit's bonds (Figure 7).[63]

Such band intensities are significantly enhanced by a factor of 15 ($azoS_2$), 30 (azo6-SAc) and 70 (azo11-SAc) in the case of azo@Au nanoassemblies compared to the azo nanospheres alone. Since correction of the laser absorption by the large number of gold nanoparticles is not taken into account, the enhancement factors should be much larger than the measured ones. They suggest that strong optical coupling exists between the AuNPs and azo core, and therefore prove the immediate proximity and anchoring of the AuNPs onto the photochromic nanospheres. Such interactions were eventually evidenced by the absence of deformation of the nanoassemblies irradiated under polarized light, which tends to confirm that the photoreactivity of molecular photochromic nanoparticles mainly proceeds from the molecules located at the surface.

CONCLUSION

In summary, stable photochromic nanoparticles have been fabricated from the bottom-up precipitation approach, involving the self-assembling of polar azo molecules in water. They undergo reversible photoreaction without dissociating owing to the stiff cohesion of molecules and show faster monoexponential relaxation toward their initial state compared to molecules dissolved in solution. Their higher photo-

DOI: 10.1021/am5076953
ACS Appl. Mater. Interfaces 2015, 7, 1932−1942

conversion yield compared to those in thin films leads to the important conclusion that larger performances of functional materials (for instance for optical data storage applications) should be achieved using matrices of nanoparticles rather than thin films constituted of molecular (or polymer) dyes. Such unexpected features were interpreted in terms of surface reactivity, as demonstrated by the elaboration of innovative plasmonic core−shell nanoassemblies azo@Au and the strong optical coupling developed between the azo surface and gold nanoparticles. Novel azo@Au nanoassemblies, expected to generate strong electric field through the creation of hot spots, are currently developed to induce directional photodeformation of the underneath azo core that would open the unexplored route toward remote organization of conductive nanoparticles.

EXPERIMENTAL SECTION

Synthesis and Chemicals. All chemical reagents and solvents were purchased from commercial sources (Aldrich, Acros, SDS) and used as received. ^{1}H and ^{13}C NMR spectra were recorded on JEOL 400 MHz spectrometer, and chemical shifts were reported in ppm relative to TMS or referenced to the residual solvent. High resolution mass spectra were obtained by MALDI-TOF (Voyager DE-STR, Applied Biosystems). Spectroscopic grade solvents purchased from Aldrich were used for spectroscopic measurements and thin film fabrication. Compound **1** was obtained following previously literature procedures.[64]

*(E)-4-((4-(Bis(4′-(tert-butyl)-[1,1′-biphenyl]-4-yl)amino)phenyl)-diazenyl)benzoyl Chloride (**2**).* The azo acid **1** (197 mg, 0.30 mmol) was dissolved in dry dichloromethane (10 mL). The solution was purged with argon, and thionyl chloride (59 mg, 0.50 mmol) was added dropwise, which immediately let the orange solution turn dark violet. After the solution was heated under reflux for 4 h, the excess thionyl chloride was removed under reduced pressure, and compound **2** was used neat in the next reaction. ^{1}H NMR (300 MHz, $CDCl_3$): δ = 8.41 (2H, d, J = 9 Hz), 8.25 (4H, multiplet), 7.67 (4H, d, J = 8.1 Hz), 7.56 (4H, d, J = 8.4 Hz), 7.50 (4H, d, J = 8.4 Hz), 7.34 (4H, d, J = 8.4 Hz), 7.18 (2H, d, J = 9 Hz), 1.37 (18H, s) ppm.

*(E)-2-Hydroxyethyl 4-((4-(Bis(4′-(tert-butyl)-[1,1′-biphenyl]-4-yl)-amino)phenyl)diazenyl)benzoate (**3**).* A solution of compound **2** (345 mg, 0.51 mmol) and ethylene glycol (10 g, 0.16 mol) in anhydrous CH_2Cl_2 (5 mL) was refluxed under argon for 18 h. After addition of water and extraction with CH_2Cl_2, the organic layer was dried over anhydrous Na_2SO_4. The solvent was removed under reduced pressure, and the resulting solid was purified by flash column chromatography on silica gel using as an eluent the mixture petroleum ether:CH_2Cl_2 4:6. Compound **3** was obtained as a bright red powder (56%, 200 mg, 0.28 mmol). ^{1}H NMR (300 MHz, $CDCl_3$): δ = 8.19 (2H, d, J = 8.7 Hz), 7.94, (2H, d, J = 8.4 Hz), 7.91 (2H, d, J = 8.7 Hz), 7.56 (4H, d, J = 8.1 Hz), 7.53 (4H, d, J = 8.1 Hz), 7.48 (4H, d, J = 8.4 Hz), 7.28 (4H, d, J = 7.5 Hz), 7.21 (2H, d, J = 8.7 Hz), 4.51 (2H, t, J = 4.5 Hz), 3.99 (2H, t, J = 4.2 Hz), 1.37 ppm (18H, s). ^{13}C NMR (75 MHz, $CDCl_3$): δ = 166.7, 156.0, 151.3, 150.9, 150.4, 147.3, 145.7, 145.6, 137.6, 137.3, 130.9, 128.2, 127.2, 126.3, 124.9, 122.5, 121.6, 67.3, 61.8, 34.9, 31.4 ppm. MALDI-HRMS $[M + H]^+$ calculated mass for $C_{47}H_{48}N_3O_3$: 702.3690 m/z. Found: 702.3682 m/z.

*(E)-2-((6-(1,2-Dithiolan-3-yl)hexanoyl)oxy)ethyl 4-((4-(Bis(4′-(tert-butyl)-[1,1′-biphenyl]-4-yl)amino)phenyl)diazenyl)benzoate (azoS$_2$) (**4**).* Compound **3** (210 mg, 0.29 mmol), lipoic acid (70 mg, 0.34 mmol) and dimethylaminopyridinium p-toluenesulfonate (DPTS) (40 g, 0.14 mmol) were dissolved in anhydrous dichloromethane (25 mL), and the resulting solution was cooled at 0 °C using an ice bath. Diisopropylcarboxydiimide (DIPC) (70 mg, 0.56 mmol) was added dropwise, and the solution color darkened. The solution was then slowly warmed up to room temperature, and stirred for an additional 2 days. After solvent removal under reduced pressure, the crude product was purified by flash column chromatography on silica gel using CH_2Cl_2 as an eluent. Compound **4** was obtained as a bright red powder (90%, 240 mg, 0.27 mmol). ^{1}H NMR (300 MHz, $CDCl_3$): δ = 8.17 (2H, d, J = 8.7 Hz), 7.93 (2H, d, J = 8.7 Hz), 7.90 (2H, d, J = 8.7 Hz), 7.56 (4H, d, J = 8.1 Hz), 7.53 (4H, d, J = 8.1 Hz), 7.49 (4H, d, J = 8.7 Hz), 7.28 (4H, d, J = 8.4 Hz), 7.21 (2H, d, J = 8.7 Hz), 4.55 (2H, multiplet), 4.45 (2H, multiplet), 3.53 (1H, multiplet), 3.12 (2H, multiplet), 2.35 (3H, multiplet), 1.87 (1H, multiplet), 1.66 (4H, multiplet), 1.47 (2H, multiplet), 1.37 ppm (18H, s). ^{13}C NMR (75 MHz, $CDCl_3$): δ = 173.4, 166.7, 156.0, 151.3, 150.4, 147.3, 145.7, 145.6, 137.6, 137.4, 130.9, 128.2, 126.6, 126.0, 125.0, 122.5, 121.6, 62.2, 61.7, 56.5, 40.9, 38.6, 34.7, 34.0, 31.5, 31.0, 28.9, 24.8 ppm. T_g = 63 °C. UV−vis (toluene, E-isomer): λ_{max} (ε) = 471 nm (27 000 mol^{-1} L cm^{-1}). MALDI-HRMS $[M + H]^+$ calculated mass for $C_{56}H_{60}N_3O_4S_2$: 890.4020 m/z. Found: 890.3980 m/z.

*(E)-6-Bromohexyl 4-((4-(Bis(4′-(tert-butyl)-[1,1′-biphenyl]-4-yl)-amino)phenyl)diazenyl)benzoate (**5**).* Compound **1** (0.4 g, 0.61 mmol), 6-bromohexan-1-ol (0.13 g, 0.72 mmol) and dimethylamino-pyridinium p-toluenesulfonate (0.08 g, 0.27 mmol) were dissolved in anhydrous dichloromethane (25 mL), and the resulting solution cooled at 0 °C using an ice bath. Diisopropylcarboxydiimide (0.15 g, 1.19 mmol) was added dropwise, and the solution color darkened. The solution was then slowly warmed up to room temperature, and stirred for an additional 2 days. After solvent removal under reduced pressure, the crude product was purified by flash column chromatography on silica gel using CH_2Cl_2 as an eluent. Compound **5** was obtained as a bright red powder (85%, 0.42 g, 0.51 mmol). ^{1}H NMR (300 MHz, $CDCl_3$): δ = 8.17 (2H, d, J = 8.5 Hz), 7.91 (2H, d, J = 8.8 Hz), 7.88 (2H, d, J = 9.1 Hz), 7.57 (4H, d, J = 8.5 Hz), 7.54 (4H, d, J = 8.3 Hz), 7.48 (4H, d, J = 8.4 Hz), 7.27 (4H, d, J = 8.7 Hz), 7.22 (2H, d, J = 8.9 Hz), 4.35 (2H, t, J = 6.6 Hz), 3.43 (2H, t, J = 6.6 Hz), 1.93 (2H, tt, J = 6.5 Hz, J = 7.0 Hz), 1.84 (2H, tt, J = 6.5 Hz, J = 7.0 Hz), 1.47 (4H, multiplet), 1.37 ppm (18H, s). ^{13}C NMR (75 MHz, $CDCl_3$): δ = 166.4, 155.8, 151.2, 150.4, 147.3, 145.7, 137.6, 137.2, 131.5, 130.7, 128.2, 126.6, 125.9, 124.9, 122.4, 121.6, 61.3, 34.7, 33.8, 32.8, 31.5, 28.7, 28.0, 25.4, ppm. MALDI-HRMS $[M + H]^+$ calculated mass for $C_{51}H_{55}BrN_3O_2$: 820.3472 m/z. Found: 820.3492 m/z.

*(E)-11-Bromoundecyl 4-((4-(Bis(4′-(tert-butyl)-[1,1′-biphenyl]-4-yl)amino)phenyl)diazenyl)benzoate (**6**).* The same procedure as that described for compound **5** was used, except that compound **1**[64] (0.22 g, 0.33 mmol), 11-bromoundecan-1-ol (0.12 g, 0.48 mmol), dimethylaminopyridinium p-toluenesulfonate (0.05 g, 0.17 mmol) and diisopropylcarboxydiimide (0.08 g, 0.63 mmol) were used. Compound **6** was obtained as a bright red powder (82%, 0.24 g, 0.27 mmol). ^{1}H NMR (300 MHz, $CDCl_3$): δ = 8.17 (2H, d, J = 8.7 Hz), 7.91 (2H, d, J = 8.7 Hz), 7.87 (2H, d, J = 9.3 Hz), 7.57 (4H, d, J = 4.8), 7.54 (4H, d, J = 4.8 Hz), 7.47 (4H, d, J = 8.7 Hz), 7.27 (4H, d, J = 8.7 Hz), 7.22 (2H, d, J = 9.0 Hz), 4.35 (2H, t, J = 6.6 Hz), 3.41 (2H, t, J = 6.6 Hz), 1.86 (2H, tt, J = 7.5 Hz, J = 7.0 Hz), 1.81 (2H, tt, J = 7.5 Hz, J = 7.0 Hz), 1.63 (2H, multiplet), 1.42 (4H, multiplet), 1.38 (18H, s), 1.30 ppm (8H, multiplet). ^{13}C NMR (75 MHz, $CDCl_3$): δ = 166.5, 155.8, 151.3, 150.5, 147.5, 145.8, 137.7, 137.4, 131.6, 130.8, 128.3, 126.7, 126.1, 125.0, 122.6, 121.8, 65.6, 34.8, 34.3, 33.1, 31.6, 29.7, 29.6, 29.0, 28.9, 28.5, 26.3, 26.2 ppm. MALDI-HRMS $[M + H]^+$ calculated mass for $C_{56}H_{65}BrN_3O_2$: 890.4255 m/z. Found: 890.4275 m/z.

*(E)-6-(Acetylthio)hexyl 4-((4-(Bis(4′-(tert-butyl)-[1,1′-biphenyl]-4-yl)amino)phenyl)diazenyl)benzoate (azo6-SAc) (**7**).* A solution of compound **5** (100 mg, 0.12 mmol) and potassium thioacetate (14 mg, 0.12 mmol) in acetone (50 mL) was stirred at room temperature for 18 h. The precipitated potassium bromide salt was filtered off, and the solution was evaporated under reduced pressure. Recrystallization from acetonitrile (25 mL) yielded compound **7** as a pure red powder (95%, 93 mg, 0.11 mmol). ^{1}H NMR (300 MHz, $CDCl_3$): δ = 8.17 (2H, d, J = 8.7 Hz), 7.91 (2H, d, J = 8.7 Hz), 7.88 (2H, d, J = 9 Hz), 7.57 (4H, d, J = 4.5 Hz), 7.55 (4H, d, J = 4.5 Hz), 7.48 (4H, d, J = 8.4 Hz), 7.27 (4H, d, J = 8.4 Hz), 7.22 (2H, d, J = 9 Hz), 4.34 (2H, t, J = 6.6 Hz), 2.90 (2H, t, J = 7.2 Hz), 2.33 (3H, s), 1.80 (2H, q, J = 6.6 Hz), 1.60 (4H, multiplet), 1.47 (2H, multiplet), 1.38 ppm (18H, s). ^{13}C NMR (75 MHz, $CDCl_3$): δ = 196.0, 166.6, 155.9, 151.4, 150.5, 147.5, 145.9, 137.8, 137.4, 131.6, 130.9, 128.3, 126.7, 126.1, 125.1, 122.6, 121.8, 65.4, 34.8, 31.6, 31.0, 29.8, 29.3, 28.9, 28.8, 25.9 ppm. T_g = 59 °C. UV−vis (toluene, E-isomer): λ_{max} (ε) = 467 nm (26 000

DOI: 10.1021/am5076953
ACS Appl. Mater. Interfaces 2015, 7, 1932−1942

mol^{-1} L cm^{-1}). MALDI-HRMS [M + H]$^+$ calculated mass for $C_{53}H_{58}N_3O_3S$: 816.4193 *m/z*. Found: 816.4170 *m/z*.

*(E)-11-(Acetylthio)undecyl 4-((4-(Bis(4′-(tert-butyl)-[1,1′-biphenyl]-4-yl)amino)phenyl)diazenyl)benzoate (azo11-SAc) (**8**).* The same procedure as that described for compound **7** was used, except that compound **6** (100 mg, 0.11 mmol) and potassium thioacetate (14 mg, 0.12 mmol) were used. The KBr salt was filtered-off, and the solution was evaporated. Recrystallization from acetonitrile (20 mL) yielded compound **7** as a pure red powder (90%, 88 mg, 0.10 mmol). ^{1}H NMR (300 MHz, $CDCl_3$): 8.16 (2H, d, *J* = 8.4 Hz), 7.92 (2H, d, *J* = 8.6 Hz), 7.88 (2H, d, *J* = 8.8 Hz), 7.64 (4H, d, *J* = 8.5 Hz), 7.57 (4H, d, *J* = 8.6 Hz), 7.54 (4H, d, *J* = 8.1 Hz), 7.46 (4H, d, *J* = 8.6 Hz), 7.27 (4H, d, *J* = 8.6 Hz), 7.21 (2H, d, *J* = 9 Hz), 4.34 (2H, t, *J* = 6.7 Hz), 2.86 (2H, t, *J* = 7.3 Hz), 2.31 (3H, s), 1.79 (2H, multiplet), 1.56 (6H, multiplet), 1.38 (18H, s), 1.28 ppm (10H, multiplet). ^{13}C NMR (75 MHz, $CDCl_3$): δ = 196.4, 166.6, 155.9, 151.4, 150.5, 147.5, 145.9, 137.8, 137.4, 131.7, 130.9, 128.3, 126.8, 126.1, 125.1, 122.6, 121.8, 65.7, 34.9, 31.7, 30.9, 29.8, 29.8, 29.6, 29.5, 29.4, 29.1, 29.0, 26.4 ppm. T_g = 40 °C. UV−vis (toluene, *E*-isomer): λ_{max} (ε) = 467 (28 000 mol^{-1} L cm^{-1}). ESI-HRMS [M + H]$^+$ calculated mass for $C_{58}H_{68}N_3O_3S$: 886.4981 *m/z*. Found: 886.4993 *m/z*.

Thin Film Fabrication. Glass plates were previously cleaned by ultrasound in a 2% alkaline solution for 30 min (Hellmanex), and rinsed with Millipore water and ethanol before drying with argon. The organic materials were spin-coated onto precleaned glass substrate using a 2 wt % azo solution in chloroform at a spin acceleration of 500 rpm/min and a speed of 1000 rpm for 2 min. The thin films were allowed to dry in the atmosphere for 24 h and stored in the dark before studying. The thicknesses were measured using a Dektak Veeco 8 profilometer.

Citrate Gold Nanoparticles AuNPs.[65] All glassware was first thoroughly cleaned with aqua regia solution (HCl:HNO_3 3:1) and rinsed three times with Millipore water. A solution of sodium citrate (0.068 g, 0.27 mmol) in Millipore water (30 mL) was heated to reflux, and cooled to 90 °C. Then, a solution of chloroauric acid ($HAuCl_4$, 0.033 g, 0.1 mmol) dissolved in Millipore water (0.2 mL) was quickly added. The mixture was vigorously stirred at 90 °C, and a color change occurred from yellow to colorless, and finally purple. After the solution was stirred for 10 min, the reaction mixture was cooled to room temperature, and any excess citrate was removed using dialysis for 12 h against Millipore water (membrane MCWO: 6−8 kDa). The gold nanoparticles were stored at 4 °C. TEM analyses provided a mean diameter of 15 ± 3 nm while UV−vis absorption measurements indicated a LSPR band, peaking at 528 nm.

Photochromic Azo Nanospheres. A stock solution of azo dyes was prepared in spectroscopy grade THF (0.2 wt %). A small aliquot (50 μL) was rapidly injected in an excess of Millipore water (2.5 mL), continuously stirred using a vortex. Precipitation of the azo compounds as nanoparticles was carried out in the dark to avoid parasite photoisomerization promoted by ambient light.

Core−Shell Nanoassemblies azo@Au. The protocol was identical to that previously described except that the azo stock solution was quickly injected into the freshly prepared solution of water-soluble citrate AuNPs, previously diluted to obtain a 0.2 wt % solution in gold material. The resulting colloidal suspension was stirred from a few hours to several days to let the ligand exchange process occur. More concentrated solutions of AuNPs did not allow us to clearly distinguish hybrid nanoassemblies, mostly masked by the large excess of gold NPs.

Nanoparticle Characterizations. Nanoparticle morphology was investigated by transmission electron microscopy (TEM, Hitachi HF2000-FEG) working at a voltage of 100 keV, using holey carbon-coated copper grids (300 mesh) to gain enough electronic contrast. The hydrodynamic diameter and size dispersion of nanoparticles were determined by dynamic light scattering (DLS) by means of a nanoparticle size analyzer Zetasizer Nano ZS ZEN 3600 (Malvern Instruments) equipped with a 4 mW He−Ne laser, operating at 633 nm, and a photomultiplier detector collecting backscattered light at an angle of 175°. Measurements were carried out at 25 °C on aqueous solutions of nano-objects. For each sample, intensity measurements were carried out in a multiacquisition mode implying automatically adjusted correlograms, and averaged measurements on 3 acquisitions. Nanoparticle mean sizes and distribution widths were obtained by fitting each correlogram with a Cumulants algorithm. Measurements of surface potential ζ were carried out by means of a Zetasizer Nano ZS ZEN 3600 (Malvern). The samples were placed in plastic cells.

Photochromism Studies. Photoisomerization of the azo samples was performed using a white light source Hg−Xe lamp (Hamamatsu − LC8) equipped with a narrow bandpass filter at 488 nm (25 nm fwmh). The absorption spectra were recorded every 10 s using a Varian Model Cary 5E spectrophotometer until no change in absorbance operated. After the samples were irradiated to the photostationary state, the rate constants of their back thermal $Z \rightarrow E$ reaction were valued from fitting the absorbance evolution at five various wavelengths as a function of time using mono- or biexponential mathematical laws. Illumination with polarized light was done using the beam of an argon ion laser (LEXEL) working at 488 nm and passing through a half-wave plate and a polarizer set horizontally. A drop of an aqueous solution of azo@Au nanoassemblies was deposited onto a TEM holey carbon-coated grid, slightly pressed onto a piece of parafilm mounted on a microscope glass slide. The glass substrate was then placed vertically so that the TEM grid was oriented normally to the incident beam while the drop was held thanks to the high surface tension provided by the underneath hydrophobic parafilm.

Raman Microscopy. Raman microscopy was performed using a Renishaw inVia Raman microscope equipped with a 785 nm line of a HPNIR diode laser, a 633 nm He−Ne line and an argon ion laser working at 457, 488 and 514 nm. The spot size of the focused laser beam on the sample using a 50× (0.75 NA) plan objective was estimated to be about 1−2 μm. The output laser power incident on the sample was fixed at 0.1% (namely 15 W·cm^{-2}) of the total energy (15 mW corresponding to 10^4 W·cm^{-2}) and the acquisition time to 1 s to obtain enough high signal-to noise ratio without damaging the samples. Each spectrum, recorded on the wavenumber range of interest [1800−900 cm^{-1}], resulted from a ten-accumulation average.

DFT Calculations. The molecular geometries were fully optimized by using the correlation functional of Lee, Yang and Parr[66] (B3LYP) with a 6-31G(d) basis as implemented in the GAUSSIAN 09 package.[67]

■ ASSOCIATED CONTENT

Supporting Information

Photoisomerization cycles of azo nanospheres. This material is available free of charge via the Internet at http://pubs.acs.org.

■ AUTHOR INFORMATION

Corresponding Author

*E. Ishow. E-mail: elena.ishow@univ-nantes.fr. Phone: +33-2-5112-5375. Fax: +33-2-5112-5402.

Author Contributions

The paper was written through contributions of all authors. All authors, Kristen E. Snell, Jean-Yves Mevellec, Bernard Humbert, François Lagugné-Labarthet, Eléna Ishow, have given approval to the final version of the paper. These authors contributed equally.

Funding

The France-Canada Research Fund and the French Ministry of Foreign Affairs are gratefully for their financial support and the funding of a France-Canada cotutelle PhD grant (K. E. Snell). The ANR n°2010 BLANC 1004-03 COME-ON of the French National Agency of Research is also strongly acknowledged for its precious financial support through the COME-ON project. F. Lagugné-Labarthet acknowledges the NSERC Discovery Grant program.

DOI: 10.1021/am5076953
ACS Appl. Mater. Interfaces 2015, 7, 1932−1942

Notes

The authors declare no competing financial interest.

■ ACKNOWLEDGMENTS

Nicolas Gautier at IMN Nantes and Julie Hemez at CEISAM Nantes are strongly acknowledged for their kind expertise in TEM measurements and mass spectra investigations, respectively.

■ REFERENCES

(1) Special Issue on Nanoplasmonics. *Chem. Soc. Rev.* **2014**, *43*, 3813−3994.
(2) Guerrero-Martínez, A.; Grzelczak, M.; Liz-Marzán, L. M. Molecular Thinking for Nanoplasmonic Design. *ACS Nano* **2012**, *6*, 3655−3662.
(3) Special Issue on Plasmonics. *Chem. Rev.* **2011**, *111*, 3667−3994.
(4) Zhang, J.; Whitesell, J. K.; Fox, M. A. Photoreactivity of Self-assembled Monolayers of Azobenzene or Stilbene Derivatives Capped on Colloidal Gold Clusters. *Chem. Mater.* **2001**, *13*, 2323−2331.
(5) Special Issue on Photochromism: Memories and Switches. *Chem. Rev.* **2000**, *100*, 1683−1890.
(6) Feringa, B. L.; Browne, W. R. *Molecular Switches*; Wiley-VCH: Weinheim, Germany, 2011; p 792.
(7) Spangenberg, A.; Metivier, R.; Yasukuni, R.; Shibata, K.; Brosseau, A.; Grand, J.; Aubard, J.; Yu, P.; Asahi, T.; Nakatani, K. Photoswitchable Interactions between Photochromic Organic Diarylethene and Surface Plasmon Resonance of Gold Nanoparticles in Hybrid Thin Films. *Phys. Chem. Chem. Phys.* **2013**, *15*, 9670−9678.
(8) Wu, B. T.; Ueno, K.; Yokota, Y.; Sun, K.; Zeng, H. P.; Misawa, H. Enhancement of a Two-Photon-Induced Reaction in Solution Using Light-Harvesting Gold Nanodimer Structures. *J. Phys. Chem. Lett.* **2012**, *3*, 1443−1447.
(9) Chang, C.-W.; Lu, Y.-C.; Wang, T.-T.; Diau, E. W.-G. Photoisomerization Dynamics of Azobenzene in Solution with S1 Excitation: A Femtosecond Fluorescence Anisotropy Study. *J. Am. Chem. Soc.* **2004**, *126*, 10109−10118.
(10) Jacquart, A.; Williams, R. M.; Brouwer, A. M.; Ishow, E. Decoupling Fluorescence and Photochromism in Bifunctional Azo Derivatives for Bulk Emissive Structures. *Chem.—Eur. J.* **2012**, *18*, 3706−3720.
(11) Poprawa-Smoluch, M.; Baggerman, J.; Zhang, H.; Maas, H. P. A.; De Cola, L.; Brouwer, A. M. Photoisomerization of Disperse Red 1 Studied with Transient Absorption Spectroscopy and Quantum Chemical Calculations. *J. Phys. Chem. A* **2006**, *110*, 11926−11937.
(12) Spangenberg, A.; Metivier, R.; Gonzalez, J.; Nakatani, K.; Yu, P.; Giraud, M.; Leaustic, A.; Guillot, R.; Uwada, T.; Asahi, T. Multiscale Approach of Photochromism: Synthesis and Photochromic Properties of a Diarylethene in Solution, in Nanoparticles, and in Bulk Crystals. *Adv. Mater.* **2009**, *21*, 309−313.
(13) Tamai, N.; Miyasaka, H. Ultrafast Dynamics of Photochromic Systems. *Chem. Rev.* **2000**, *100*, 1875−1890.
(14) Nishi, H.; Asahi, T.; Kobatake, S. Plasmonic Enhancement of a Photocycloreversion Reaction of a Diarylethene Derivative Using Individually Dispersed Silver Nanoparticles. *ChemPhysChem* **2012**, *13*, 3616−3621.
(15) Ouhenia-Ouadahi, K.; Yasukuni, R.; Yu, P.; Laurent, G.; Pavageau, C.; Grand, J.; Guerin, J.; Leaustic, A.; Felidj, N.; Aubard, J.; Nakatani, K.; Metivier, R. Photochromic-Fluorescent-Plasmonic Nanomaterials: Towards Integrated Three-Component Photoactive Hybrid Nanosystems. *Chem. Commun.* **2014**, *50*, 7299−7302.
(16) Nishi, H.; Asahi, T.; Kobatake, S. Plasmonic Enhancement of Gold Nanoparticles on Photocycloreversion Reaction of Diarylethene Derivatives Depending on Particle Size, Distance from the Particle Surface, and Irradiation Wavelength. *Phys. Chem. Chem. Phys.* **2012**, *14*, 4898−4905.
(17) Baudrion, A.-L.; Perron, A.; Veltri, A.; Bouhelier, A.; Adam, P.-M.; Bachelot, R. Reversible Strong Coupling in Silver Nanoparticle Arrays Using Photochromic Molecules. *Nano Lett.* **2013**, *13*, 282−286.
(18) Grzelczak, M.; Perez-Juste, J.; Mulvaney, P.; Liz-Marzan, L. M. Shape Control in Gold Nanoparticle Synthesis. *Chem. Soc. Rev.* **2008**, *37*, 1783−1791.
(19) Irie, M. Diarylethenes for Memories and Switches. *Chem. Rev.* **2000**, *100*, 1685−1716.
(20) Yamaguchi, H.; Matsuda, K.; Irie, M. Excited-State Behavior of a Fluorescent and Photochromic Diarylethene on Silver Nanoparticles. *J. Phys. Chem. C* **2007**, *111*, 3853−3862.
(21) Nishi, H.; Asahi, T.; Kobatake, S. Enhanced Photocycloreversion Reaction of Diarylethene Polymers Attached to Gold Nanoparticles in the Solid State. *J. Photochem. Photobiol., A* **2011**, *221*, 256−260.
(22) Shiraishi, Y.; Tanaka, K.; Shirakawa, E.; Sugano, Y.; Ichikawa, S.; Tanaka, S.; Hirai, T. Light-Triggered Self-Assembly of Gold Nanoparticles Based on Photoisomerization of Spirothiopyran. *Angew. Chem., Int. Ed.* **2013**, *52*, 8304−8308.
(23) Ipe, B. I.; Mahima, S.; Thomas, K. G. Light-Induced Modulation of Self-Assembly on Spiropyran-Capped Gold Nanoparticles: A Potential System for The Controlled Release of Amino Acid Derivatives. *J. Am. Chem. Soc.* **2003**, *125*, 7174−7175.
(24) Rau, H. Azo Compounds. In *Photochromism, Molecules and Systems*; Dürr, H., Bouas-Laurent, H. , Eds.; Elsevier: Amsterdam, 2003; pp 165−188.
(25) Ichimura, K.; Oh, S.-K.; Nakagawa, M. Light-Driven Motion of Liquids on a Photoresponsive Surface. *Science* **2000**, *288*, 1624−1626.
(26) Diguet, A.; Guillermic, R.-M.; Magome, N.; Saint-Jalmes, A.; Chen, Y.; Yoshikawa, K.; Baigl, D. Photomanipulation of a Droplet by the Chromocapillary Effect. *Angew. Chem., Int. Ed.* **2009**, *121*, 9361−9361.
(27) Kausar, A.; Nagano, H.; Ogata, T.; Nonaka, T.; Kurihara, S. Photocontrolled Translational Motion of a Microscale Solid Object on Azobenzene-Doped Liquid-Crystalline Films. *Angew. Chem., Int. Ed.* **2009**, *48*, 1−5.
(28) Manna, A.; Chen, P.-L.; Akiyama, H.; Wei, T.-X.; Tamada, K.; Knoll, W. Optimized Photoisomerization on Gold Nanoparticles Capped by Unsymmetrical Azobenzene Disulfides. *Chem. Mater.* **2002**, *15*, 20−28.
(29) Klajn, R.; Wesson, P. J.; Bishop, K. J. M.; Grzybowski, B. A. Writing Self-Erasing Images Using Metastable Nanoparticle "Inks". *Angew. Chem., Int. Ed.* **2009**, *48*, 7035−7039.
(30) Das, S.; Ranjan, P.; Maiti, P. S.; Singh, G.; Leitus, G.; Klajn, R. Dual-Responsive Nanoparticles and Their Self-Assembly. *Adv. Mater.* **2013**, *25*, 422−426.
(31) Yoon, J. H.; Yoon, S. Photoisomerization of Azobenzene Derivatives Confined in Gold Nanoparticle Aggregates. *Phys. Chem. Chem. Phys.* **2011**, *13*, 12900−12905.
(32) Priimagi, A.; Shevchenko, A. Azopolymer-based Micro- and Nanopatterning for Photonic Applications. *J. Polym. Sci., Part B: Polym. Phys.* **2014**, *3*, 163−182.
(33) Galarreta, B. C.; Rupar, I.; Young, A.; Lagugne-Labarthet, F. Mapping Hot-Spots in Hexagonal Arrays of Metallic Nanotriangles with Azobenzene Polymer Thin Films. *J. Phys. Chem. C* **2011**, *115*, 15318−15323.
(34) Konig, T.; Yadavalli, N. S.; Santer, S. Near-Field Induced Reversible Structuring of Photosensitive Polymer Films: Gold versus Silver Nano-antennas. *Plasmonics* **2012**, *7*, 535−542.
(35) Torres, T.; Bottari, G. *Organic Nanomaterials: Synthesis, Characterization, and Device Applications*; John Wiley & Sons, Inc.: Hoboken, NJ, 2013; p 622.
(36) Zhang, J.; Zou, Q.; Tian, H. Photochromic Materials: More than Meets the Eye. *Adv. Mater.* **2013**, *25*, 378−399.
(37) Asahi, T.; Sugiyama, T.; Masuhara, H. Laser Fabrication and Spectroscopy of Organic Nanoparticles. *Acc. Chem. Res.* **2008**, *41*, 1790−1798.
(38) Kim, S.; Yoon, S.-J.; Park, S. Y. Highly Fluorescent Chameleon Nanoparticles and Polymer Films: Multicomponent Organic Systems that Combine FRET and Photochromic Switching. *J. Am. Chem. Soc.* **2012**, *134*, 12091−12097.

DOI: 10.1021/am5076953
ACS Appl. Mater. Interfaces 2015, 7, 1932−1942

(39) Patra, A.; Metivier, R.; Brisset, F.; Nakatani, K. Photochromic One-Dimensional Nanostructures Based on Dithienylethene: Fabrication by Light-Induced Precipitation and Reversible Transformation in the Nanoparticle State. *Chem. Commun.* **2012**, *48*, 2489−2491.
(40) Han, M.; Hara, M. Intense Fluorescence from Light-Driven Self-Assembled Aggregates of Nonionic Azobenzene Derivative. *J. Am. Chem. Soc.* **2005**, *127*, 10951−10955.
(41) Han, M. R.; Hashizume, D.; Hara, M. Self-Assembly of Long-Lived *cis*-Azobenzenes into Crystalline Nanoparticles. *New J. Chem.* **2007**, *31*, 1746−1750.
(42) Pelaz, B.; Jaber, S.; de Aberasturi, D. J.; Wulf, V.; Aida, T.; de la Fuente, J. M.; Feldmann, J.; Gaub, H. E.; Josephson, L.; Kagan, C. R.; Kotov, N. A.; Liz-Marzan, L. M.; Mattoussi, H.; Mulvaney, P.; Murray, C. B.; Rogach, A. L.; Weiss, P. S.; Willner, I.; Parak, W. J. The State of Nanoparticle-Based Nanoscience and Biotechnology: Progress, Promises, and Challenges. *ACS Nano* **2012**, *6*, 8468−8483.
(43) Hassan, N.; Cabuil, V.; Abou-Hassan, A. Continuous Multistep Microfluidic Assisted Assembly of Fluorescent, Plasmonic, and Magnetic Nanostructures. *Angew. Chem., Int. Ed.* **2013**, *52*, 1994−1997.
(44) Wang, F.; Richards, V. N.; Shields, S. P.; Buhro, W. E. Kinetics and Mechanisms of Aggregative Nanocrystal Growth. *Chem. Mater.* **2014**, *26*, 5−21.
(45) Faucon, A.; Lenk, R.; Hemez, J.; Gautron, E.; Jacquemin, D.; Le Questel, J.-Y.; Graton, J.; Brosseau, A.; Ishow, E. Fluorescent Carboxylic and Phosphonic Acids: Comparative Photophysics from Solution to Organic Nanoparticles. *Phys. Chem. Chem. Phys.* **2013**, *15*, 12748−12756.
(46) Balan, B.; Vijayakumar, C.; Ogi, S.; Takeuchi, M. Oligofluorene-based Nanoparticles in Aqueous Medium: Hydrogen Bond Assisted Modulation of Functional Properties and Color Tunable FRET Emission. *J. Mater. Chem.* **2012**, *22*, 11224−11234.
(47) Roger, K.; Cabane, B. Why Are Hydrophobic/Water Interfaces Negatively Charged? *Angew. Chem., Int. Ed.* **2012**, *51*, 5625−5628.
(48) Nakano, H.; Takanashi, T.; Kadota, T.; Shirota, Y. Formation of Surface Relief Grating Using a Novel Azobenzene-based Photochromic Amorphous Molecular Material. *Adv. Mater.* **2002**, *14*, 1157−1160.
(49) Ishow, E.; Lebon, B.; He, Y. N.; Wang, X. G.; Bouteiller, L.; Galmiche, L.; Nakatani, K. Structural and Photoisomerization Cross Studies of Polar Photochromic Monomeric Glasses Forming Surface Relief Gratings. *Chem. Mater.* **2006**, *18*, 1261−1267.
(50) Bahrenburg, J.; Renth, F.; Temps, F.; Plamper, F.; Richtering, W. Femtosecond Spectroscopy Reveals Huge Differences in the Photoisomerisation Dynamics between Azobenzenes Linked to Polymers and Azobenzenes in Solution. *Phys. Chem. Chem. Phys.* **2014**, *16*, 11549−11554.
(51) Dokić, J.; Gothe, M.; Wirth, J.; Peters, M. V.; Schwarz, J.; Hecht, S.; Saalfrank, P. Quantum Chemical Investigation of Thermal Cis-to-Trans Isomerization of Azobenzene Derivatives: Substituent Effects, Solvent Effects, and Comparison to Experimental Data. *J. Phys. Chem. A* **2009**, *113*, 6763−6773.
(52) Yasukuni, R.; Sliwa, M.; Hofkens, J.; De Schryver, F. C.; Herrmann, A.; Mullen, K.; Asahi, T. Size-Dependent Optical Properties of Dendronized Perylenediimide Nanoparticle Prepared by Laser Ablation in Water. *Jpn. J. Appl. Phys.* **2009**, *48*, 065002.
(53) Faucon, A.; Fresnais, J.; Brosseau, A.; Hulin, P.; Nedellec, S.; Hemez, J.; Ishow, E. Photoactive Chelating Organic Nanospheres as Central Platforms of Bimodal Hybrid Nanoparticles. *J. Mater. Chem. C* **2013**, *1*, 3879−3886.
(54) Breton, M.; Prevel, G.; Audibert, J. F.; Pansu, R.; Tauc, P.; Le Pioufle, B.; Francais, O.; Fresnais, J.; Berret, J. F.; Ishow, E. Solvatochromic Dissociation of Non-Covalent Fluorescent Organic Nanoparticles upon Cell Internalization. *Phys. Chem. Chem. Phys.* **2011**, *13*, 13268−13276.
(55) Tong, X.; Wang, G.; Zhao, Y. Photochemical Phase Transition versus Photochemical Phase Separation. *J. Am. Chem. Soc.* **2006**, *128*, 8746−8747.
(56) Klajn, R.; Bishop, K. J. M.; Grzybowski, B. A. Light-Controlled Self-Assembly of Reversible and Irreversible Nanoparticle Suprastructures. *Proc. Natl. Acad. Sci. U. S. A.* **2007**, *104*, 10305−10309.
(57) Tong, X.; Wang, G.; Soldera, A.; Zhao, Y. How Can Azobenzene Block Copolymer Vesicles Be Dissociated and Reformed by Light? *J. Phys. Chem. B* **2005**, *109*, 20281−20287.
(58) Vecchi, I.; Arcioni, A.; Bacchiocchi, C.; Tiberio, G.; Zanirato, P.; Zannoni, C. Expected and Unexpected Behavior of the Orientational Order and Dynamics Induced by Azobenzene Solutes in a Nematic. *J. Phys. Chem. B* **2007**, *111*, 3355−3362.
(59) Li, Y.; He, Y.; Tong, X.; Wang, X. Photoinduced Deformation of Amphiphilic Azo Polymer Colloidal Spheres. *J. Am. Chem. Soc.* **2005**, *127*, 2402−2403.
(60) Li, Y.; He, Y.; Tong, X.; Wang, X. Stretching Effect of Linearly Polarized Ar^+ Laser Single-Beam on Azo Polymer Colloidal Spheres. *Langmuir* **2006**, *22*, 2288−2291.
(61) Wang, Y.; Bing, Yan; Chen, L. SERS Tags: Novel Optical Nanoprobes for Bioanalysis. *Chem. Rev.* **2013**, *113*, 1391−1428.
(62) Boubekri, R.; Yasukuni, R.; Truong, S. L.; Grand, J.; Perrier, A.; Aubard, J.; Maurel, F. Raman Study of A Photochromic Diarylethene Molecule: A Combined Theoretical and Experimental Study. *J. Raman Spectrosc.* **2013**, *44*, 1777−1785.
(63) Marquestaut, N.; Martin, A.; Talaga, D.; Servant, L.; Ravaine, S.; Reculusa, S.; Bassani, D. M.; Gillies, E.; Lagugné-Labarthet, F. Raman Enhancement of Azobenzene Monolayers on Substrates Prepared by Langmuir-Blodgett Deposition and Electron-Beam Lithography Techniques. *Langmuir* **2008**, *24*, 11313−11321.
(64) Snell, K. E.; Stéphant, N.; Pansu, R. B.; Audibert, J.-F.; Lagugné-Labarthet, F.; Ishow, E. Nanoparticle Organization through Photoinduced Bulk Mass Transfer. *Langmuir* **2014**, *30*, 2926−2935.
(65) Ojea-Jiménez, I.; Bastús, N. G.; Puntes, V. Influence of the Sequence of the Reagents Addition in the Citrate-Mediated Synthesis of Gold Nanoparticles. *J. Phys. Chem. C* **2011**, *115*, 15752−15757.
(66) Barone, V.; Polimeno, A. Integrated Computational Strategies for UV/vis Spectra of Large Molecules in Solution. *Chem. Soc. Rev.* **2007**, *36*, 1724−1731.
(67) Frisch, M. J. et al. *Gaussian 09*, Revision A.02; Gaussian Inc.: Wallingford, CT, 2013.

DOI: 10.1021/am5076953
ACS Appl. Mater. Interfaces 2015, 7, 1932−1942